A Vortex-Free Flexible Turbine Blade for Wave Energy Conversion: Model, Design, and Preliminary Test Results[1]

Asfaw Beyene

Department of Mechanical Engineering
San Diego State University
San Diego, CA 92128, USA, abeyene@sdsu.edu

Abstract:

The Wells turbine is an axial-flow, self-rectifying turbine widely used for converting wave energy into electrical power. Numerous strategies have been proposed to improve its performance, including geometric modifications, aerodynamic optimization of blade angles, counter-rotating biplane configurations, and variable-pitch mechanisms. Although these methods can enhance efficiency under specific conditions, the performance of Wells turbines remains highly sensitive to part-load operation. This study build uses a previously introduced flexible turbine blade and adds a twist to render the design vortex free. The new designs were modeled and tested using a low-speed wind tunnel. Experimental results show that the vortex-free blade significantly outperforms the standard Wells turbine under variable load conditions. The new blade achieved a peak efficiency of 82% and exhibited substantially improved part-load performance compared with the conventional Wells turbine with estimated maximum efficiency typically about 70%.

Keywords:

Wave energy; Well's turbine; Flexible blade; Energy; Sustainability.

1. Introduction

The Wells turbine, invented by A. A. Wells in 1984 through a joint research program with Queen's University Belfast [1], is the most widely used turbine in oscillating water column (OWC) wave-energy systems. OWCs convert the oscillatory motion of waves into a bi-directional airflow that drives a turbine–generator system, [2]. Several full-scale installations, including a 75-kW unit in Islay, Scotland and two 500 kW units in Pico, Azores, have demonstrated the technology's potential [3].

The turbine consists of multiple symmetrical airfoil blades mounted on a rotor, Fig. 1. As the oscillating airflow reverses direction, the incidence angle also reverses in sign, but the tangential force always acts in the same rotational direction due to blade symmetry. Thus, the Wells turbine self-rectifies, eliminating the need for mechanical valves.

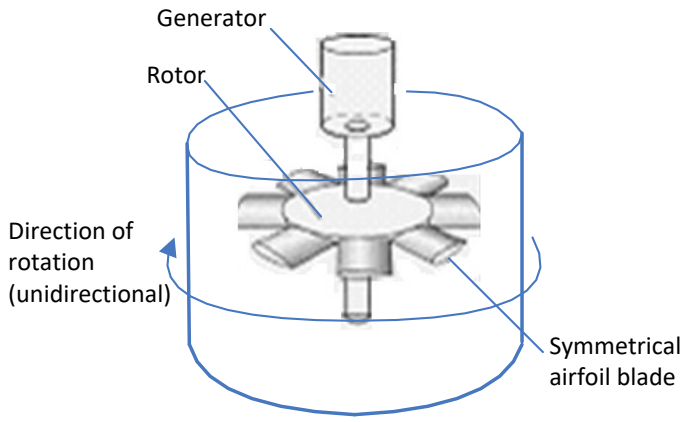

[1] This paper is extracted from the M.Sc. thesis of the late Dhananjay Mangalekar, my graduate student, in whose honor it is dedicated and preserved.

Figure 1. Wells turbine

A representative performance curve of the turbine is shown on Fig. 2. Aerodynamic efficiency, η_a, depends strongly on the incidence angle (and thus on the flow ratio Φ). Efficiency is low at small incidence angles—typical of part-load operation—and decreases again at high incidence angles due to stall. Because ocean waves vary continuously in amplitude, the associated airflow fluctuates widely, giving Wells turbines a narrow effective operating range.

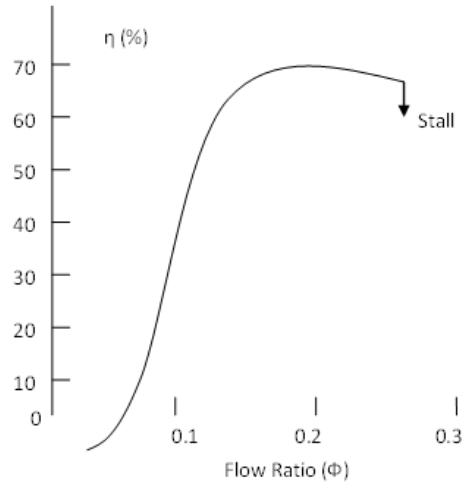

Figure 2. Typical performance curve for a Wells Turbine.

A variety of strategies have been explored to improve performance [4], including leading-edge slats, trailing-edge modifications, thick airfoils, and offset blades. While these may delay stall, they often reduce peak efficiency and do not address the fundamental limitation: poor part-load performance.

Biological Inspiration: marine animals achieve high propulsive efficiency through precise vorticity control [5, 6]. Fish fins undergo controlled twisting and bending, preventing premature flow separation and suppressing vortex shedding. This principle motivates the exploration of flexible blades for Wells turbines, with the goal of regulating the local angle of attack under varying aerodynamic loads.

Research Objective: this work investigates two adaptive-blade turbine concepts:

- Flexible turbine that bends elastically near the trailing edge, with blades made from a compliant material adjusting their effective exit angle β_2 under load.

- Free vortex design, by varying blade thickness along the span, thinnest at the tip, the blade undergoes controlled twisting and bending near the trailing edge under different loading conditions. This produces vortex-free flow near the blade tips, reducing tip losses while preserving the benefits of the flexible-blade concept described above.

Both designs are compared to the standard Wells turbine via mathematical modeling and wind-tunnel experiments.

2. Mathematical Model

The mathematical modeling is organized as follows:
a. Velocity diagrams for the standard Wells turbine
b. Modeling of the flexible-turbine concept
c. Modeling of the vortex-free (variable-thickness to allow twist) blade

2.1. Velocity Diagram for Standard Wells Turbine

Figure 3 presents the inlet and outlet velocity triangles. These relations provide the basis for modeling both the standard and modified designs.

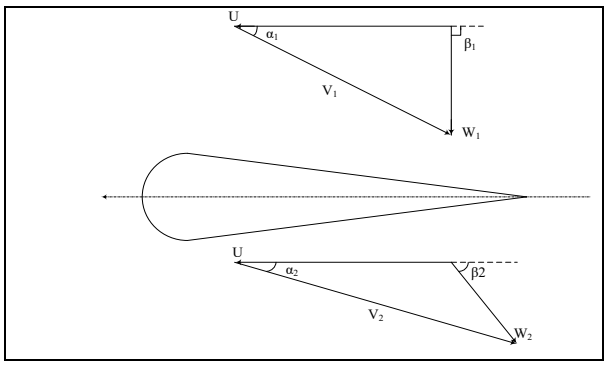

Figure 3. Inlet and outlet velocity triangles for a standard Wells turbine, [7].

2.2. Manuscript submission and review process

The following specifications were used, Fig. 4, to design the blade:

N = 1200 rpm
ω = 125.66 rad/s
n = 5 blades
$\beta_1 = 90°$
P = 20 W
ID = 0.2032 m

$D_{tip} = 0.200$ m
$D_{hub} / D_{tip} = 0.6$
$D_{hub} = 0.120$ m
h = 0.04 m
$\rho_{air} = 1.225$ kg/m³.

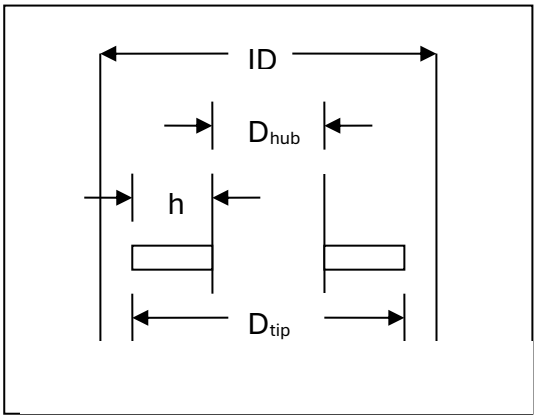

Figure 4. Turbine dimensions, [7].

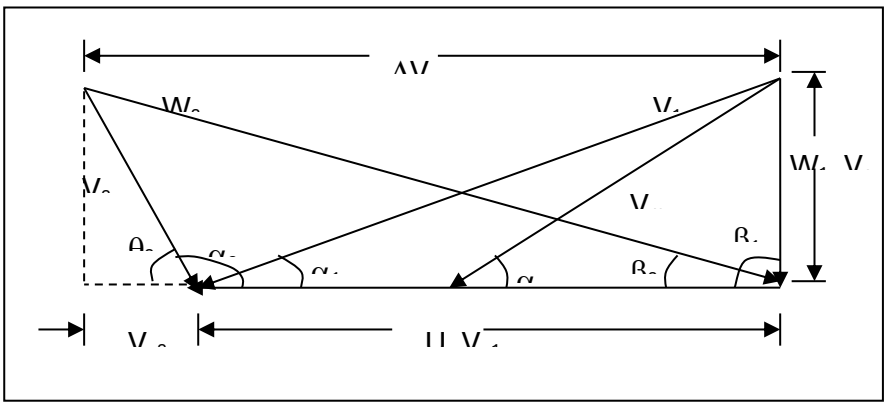
Figure 5. Velocity diagram with β2 < α1, [7].

Velocity Triangles and Derivations: The flexible design allows β_2 to vary with load, leading to two configurations, [7]:

$\beta_2 < \alpha_1$ (Eqs 1–7)	**$\beta_2 > \alpha_1$** (Eqs 9–18)
$U = V_{u1}, W_1 = V_a, V_m = \frac{W_1}{\sin \alpha_m}$ (1)	$U = V_{u1}, W_1 = V_a, V_m = \frac{W_1}{\sin \alpha_m}$ (9)
$\tan \alpha_1 = \frac{W_1}{U}, \quad \therefore W_1 = U \tan \alpha_1$ (2)	$\tan \alpha_1 = \frac{W_1}{U}, \quad \therefore W_1 = U \tan \alpha_1$ (10)
$\cos \alpha_1 = \frac{U}{V_1}, \quad \therefore V_1 = U \cos \alpha_1$ (3)	$\cos \alpha_1 = \frac{U}{V_1}, \quad \therefore V_1 = U \cos \alpha_1$ (11)
$\tan \beta_2 = \frac{W_1}{\Delta V_u}, \therefore \Delta V_u = \frac{W_1}{\tan \beta_2}$ (4)	$\sin \beta_2 = \frac{W_1}{W_2}, \therefore W_2 = \frac{W_1}{\sin \beta_2}$ (12)
$\Delta V_u = V_{u1} + V_{u2}, \therefore V_{u2} = \Delta V_u - V_{u1}$ (5)	$\cos \beta_2 = \frac{\Delta V_u}{W_2}, \therefore \Delta V_u = W_2 \cos \beta_2$ (13)
$\sin \beta_2 = \frac{W_1}{W_2}, \therefore W_2 = \frac{W_1}{\sin \beta_2}$ (6)	$\Delta V_u = V_{u1} - V_{u2}, \therefore V_{u2} = V_{u1} - \Delta V_u$ (14)
$V_2 = W_1^2 - V_{u2}^2, \therefore V_2 = \sqrt{W_1^2 + V_{u2}^2}$ (7)	$V_2 = W_1^2 - V_{u2}^2, \therefore V_2 = \sqrt{W_1^2 + V_{u2}^2}$ (15)
	$\tan \alpha_2 = \frac{W_1}{V_{u2}}, \therefore \alpha_2 = tan^{-1} \frac{W_1}{V_{u2}}$ (16)
	$\cos \alpha_2 = \frac{V_{u2}}{V_2}, \therefore V_2 = \frac{V_{u2}}{\cos \alpha_2}$ (17)
	$\tan \alpha_m = \frac{2(W_1)}{V_{u1}+V_{u2}}, \therefore \alpha_m = tan^{-1} \frac{2(W_1)}{V_{u1}+V_{u2}}$ (18)

These sets of relations were used to compute the velocity components, Fig. 5, and resulting forces.

Airfoil Selection: Using the design specifications, optimal performance occurs at an incidence angle $\alpha_1 = 7°$, corresponding to the highest lift-to-drag ratio (Cl/Cd ≈ 58.6) for a NACA 1412 airfoil (Fig. 6).

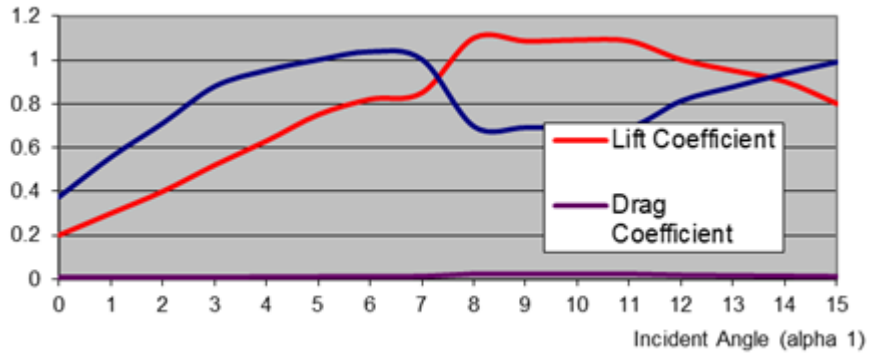

Figure 6. Lift and drag coefficients for NACA 1412 airfoils, [7]

Force Relations

The lift force:

$$A = \frac{1}{2} \cdot C_l \cdot \rho \cdot {V_m}^2 \cdot C \cdot h \quad (19)$$

Tangential thrust:

$$T = \dot{m}\, \Delta V_u = Sh\rho W_1 \Delta V_u \quad (20)$$

Neglecting drag, equating the two forms yields:

$$\Delta V_u = \frac{C_L}{2} \frac{c}{S} \frac{W_1}{\sin \alpha_m} \quad (21)$$

The pressure drop follows from Euler's turbine equation:

$$\Delta p = \rho U \Delta V_u \quad (22)$$

Chord Length Constraint

Geometric constraints at the hub and mean radius yield:

$$C = \frac{0.5027}{5(1+S/C)} \quad (23)$$

Equation (23) gives the available chord length for each β2 variation. The tangential thrust on each blade is then calculated. The theoretical power P that can be generated by the turbine for each variation of β2 is obtained using

$$P = nTU \quad (24)$$

2.3. Mathematical Modeling for free-vortex (Variable Thickness) scenario

As shown above, the flexible turbine exhibits better performance than the conventional Wells turbine. This section presents an enhancement to the flexible turbine through the incorporation of a flexible blade design. In this approach, the airfoil geometry is modified to achieve no vortex formation at the blade tip, thereby reducing the energy losses caused by tip vortices. The central idea behind the vortex-free concept is that the tangential force should remain uniform along the blade span. Maintaining a constant tangential force ensures a uniform distribution of energy, which suppresses vortex formation near the tip. This is achieved by designing an airfoil with a spanwise variation in the trailing-edge angle β_2. This requires imposing a specific radial variation of the trailing-edge angle β_2, derived using the radial equilibrium method, [8, 9].

Radial Equilibrium: assuming axisymmetric flow and negligible radial velocity:

$$\frac{1}{\rho}\frac{dp}{dr} = \frac{V_u^2}{r} \quad (25)$$

The stagnation pressure condition leads to the classical radial equilibrium equation:

$$\frac{d(V_a^2)}{dr} + \frac{1}{r^2}\frac{d(rV_u)^2}{dr} = 0 \quad (26)$$

Free-Vortex Design Condition: A vortex-free condition requires $rV_u =$ constant. Substituting into the radial equilibrium equation gives a constant axial velocity. Using the inlet and outlet vortex constants (C_1, C_2):

$$\tan\ \beta_2 = \frac{rV_a}{C_1+C_2} \quad (27)$$

Thus:

$$\beta_2 = \tan^{-1}\left(\frac{rV_a}{C_1+C_2}\right) \quad (28)$$

Using values derived from the flexible-turbine optimum (V_{u1} = 10.05 m/s, V_{u2} = 3.1 m/s), β_2 varies from 0° at the hub to 10° at the tip. This forms the basis of the variable-thickness blade geometry.

3. Blade manufacturing

The manufacturing process involved creating CAD models of turbine casing, generator housing, rotor, and blades, as well as the molds required for blade fabrication. The geometrical dimensions used in the CAD models were developed in Pro/E Wildfire from the mathematical modeling described earlier. These CAD drawings were subsequently used to manufacture the turbine components and molds. The molds were employed to produce the rigid Wells turbine blades and the flexible turbine blades. Injection molding was used to fabricate a modular “sandwich rotor” enabling rapid swapping of blade prototypes.

Two blade categories were fabricated:

a) **Constant thickness (NACA 0012):**
   - Rigid (QuickCast) for standard Wells turbine
   - Flexible versions (RU-470 and RU-455)

b) **Vortex-free,** i.e., the blade thickness decreases progressively from root to tip, maximum at the root and minimum at the tip. This configuration, illustrated in Figure 9, is referred to as the variable-thickness design. Owing to its thickness variation, the blade undergoes twist at the trailing edge under aerodynamic loading, providing the spanwise variation in trailing-edge angle β_2 necessary for vortex-

free flow. Mathematical modeling predicted that a β_2 variation (twist) of approximately 10° would achieve vortex suppression at the tip, [10].

Because it is not feasible to predict the exact twist behavior of a real blade without experimentation, three different geometric variations of the variable-thickness blade were designed: (40%, 50%, 60% tip-thickness reduction). Each made of the blades was made of two materials giving a total of six variants.

CNC-milled acrylic molds were produced based on the CAD models. Urethane/silicone materials were chosen after evaluation of flexibility, pourability, and durability. A total of 60 blades were successfully manufactured. Figure 7 illustrates the arrangement of the generator housing and rotor.

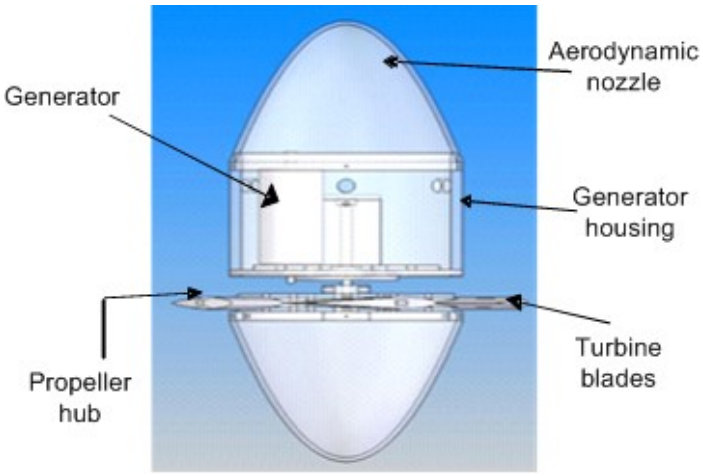

Figure 7. Arrangement of generator housing and rotor, [7].

4. Testing

The turbine was mounted on two fixtures inside the wind tunnel. Upstream, the turbine casing was secured to a fixture with two jaws, which were connected to the casing via two wooden pieces and setscrews; the wooden pieces were glued to the casing. Downstream, the generator housing was supported on a motor-actuated fixture capable of vertical movement. This fixture allowed precise leveling of the turbine so that the airflow was perpendicular to the blades, verified using a digital level.

The DC motor in the generator housing was connected to a 10-ohm resistor, and a Fluke voltmeter was used to measure the voltage across the resistor. Wind speed was measured with a digital anemometer, and turbine speed was measured using a strobe tachometer.

Testing began with the rigid blades of the standard Wells turbine (Design R). The blades were mounted on the rotor, and the wind tunnel was gradually ramped up until the turbine started rotating. At this point, the wind speed, voltage, and turbine speed were recorded. Six to seven readings were taken at different airflow rates, with testing performed up to a maximum speed of 2100 rpm. Higher speeds were avoided due to the fragile nature of the acrylic structure.

All other blade designs were tested in a similar manner, and readings were collected for the same airflow rates as used for the rigid blades.

During dynamic testing, it was not possible to directly measure the bend of flexible blades or the combined bend and twist of the vortex-free blade designs. To address this, a static testing setup was created, consisting of a special fixture to hold a single blade in the wind tunnel.

- Flexible blades (Designs F1 and F2) were tested for bend.
- Vortex-free designs (V1–V6) were tested for both bend and twist.

For each design, a blade was mounted on the fixture, and airflow was varied to match the conditions used during dynamic testing. The resulting bend and twist were captured using a high-resolution digital camera. The photographs were then printed on grid paper, and the bend and twist were calculated trigonometrically.

5. Results

Power and deformation characteristics were evaluated for all nine blade designs.

Key Findings:

- **Flexible designs (F1, F2):** F2 (more flexible) produced higher power and bend, performing significantly better at low airflow rates.
- **Vortex-free blade designs (V1–V6):** Design **V4** (50% thickness reduction, RU-455 material) achieved the highest efficiency.

Overall, the vortex-free blade outperformed both the standard Wells turbine and the flexible turbine across all flow rates (Figures 8 and 9).

As shown in Fig. 8, the performance of the vortex-free blade design is superior to that of the other two designs (standard Wells turbine and flexible turbine). The vortex-free design generates more power at full load than the flexible design and performs much better in part-load conditions (i.e., low airflow conditions).

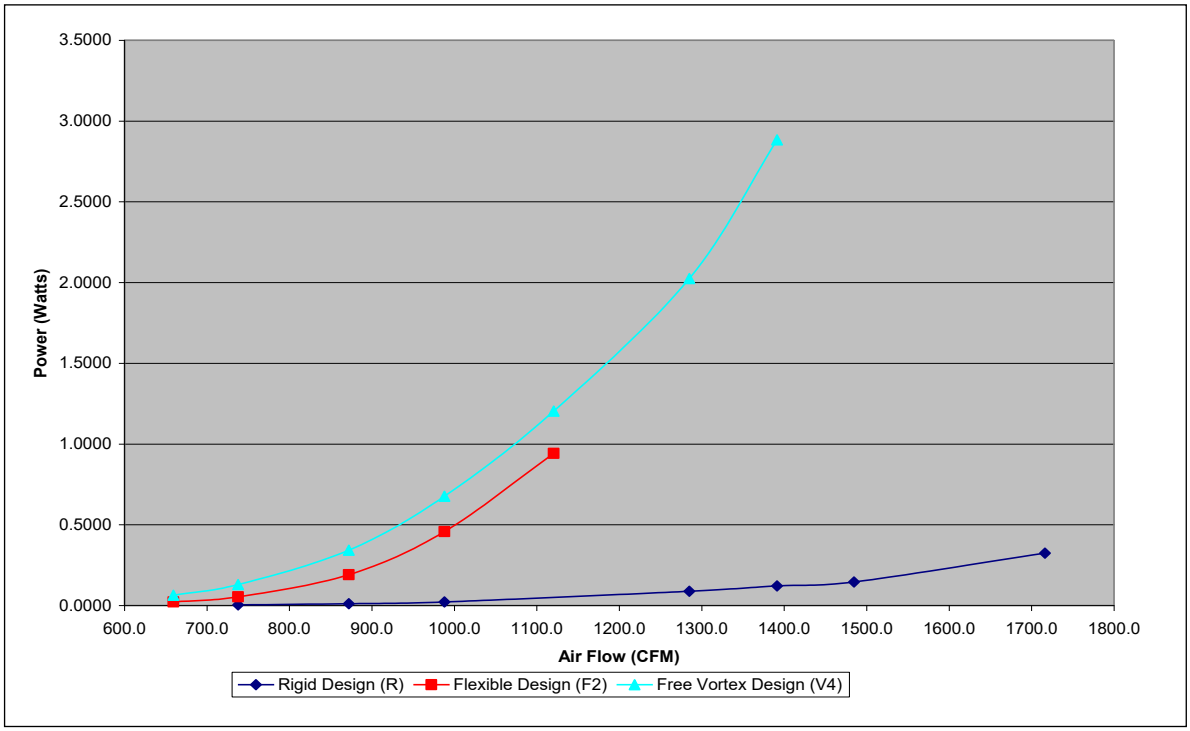

Figure 8. Comparison of power generated (Wells, flexible, vortex free designs), [7].

Figure 9 compares the turbine speed for the three designs mentioned above. As seen from the graph, , the performance of Free Vortex design was found to be superior of all three designs (i.e. standard Wells turbine, flexible turbine and free-vortex turbine). This design generated more power at full load compared to the flexible design and performed much better in part-load conditions (i.e. low air flow conditions). The speed of flexible turbines is more than that of vortex-free turbines for the same air flow rates, but the power generated by vortex-free turbines is more. This proves that the vortex-free blades generate more torque (or extract more energy) over the same flow rate, hence the blades of vortex-free design are more efficient compared to the flexible design.

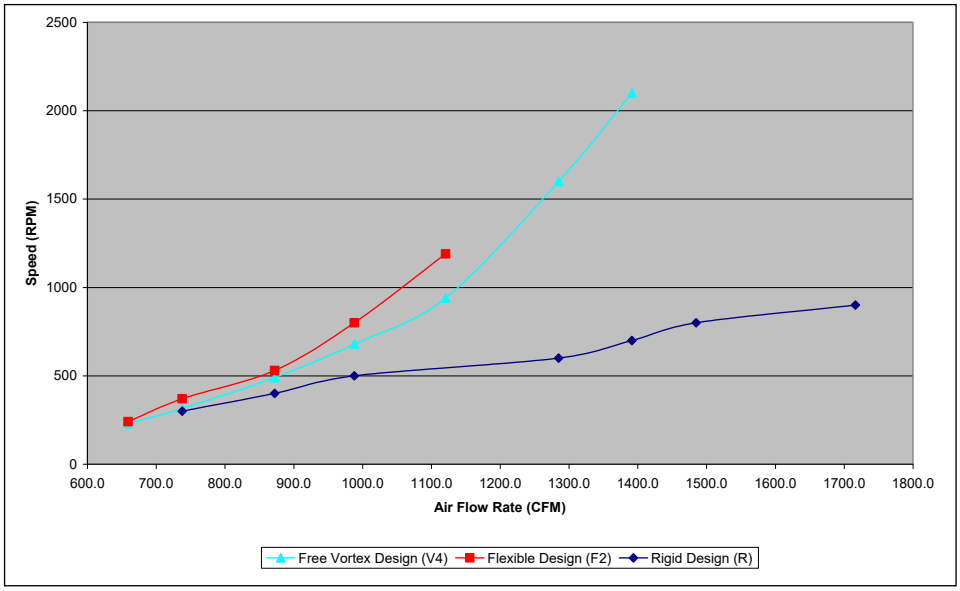

Figure 9. Comparison of turbine speed (Wells, flexible, and vortex-free turbine blades), [7].

Design V4 achieved the highest efficiency at ~82%, significantly exceeding the standard Wells turbine (≈70%) and the flexible turbine (≈75–78%) efficiencies.

6. Conclusion

The Wells turbine is a key component in wave energy conversion but suffers from limited operating range and low part-load efficiency. To address these limitations, flexible and vortex-free flexible-blade turbine designs were developed and tested, showing significant improvements over the standard design. This work demonstrates that adaptive blade flexibility—implemented via bending trailing edges and spanwise twist—offers a powerful method for improving Wells turbine performance. Both the flexible and the vortex-free turbines significantly outperform the conventional design in the part-load regime. The vortex-free, i.e., variable-thickness flexible blade, particularly design V4, delivered the best performance, offering:

- Higher torque
- Greater power output
- Suppressed vortex losses
- Peak efficiency of ≈82%

The flexible turbine features blades with trailing edges that bend in response to load. Mathematical modeling predicted a 1.9-fold increase in peak power compared to the standard turbine, which was confirmed by wind tunnel tests. Power output was found to be proportional to trailing-edge bend, validating the design approach.

The twist compounded flexible-blade further enhances performance by eliminating tip vortices through variable-thickness blades. These blades taper from a thick root to a thin tip, producing trailing-edge twist and bend under load to maintain vortex-free flow. Among six prototypes tested, design V4 achieved the highest efficiency (82% at full load) and superior part-load performance, producing 3 W of power with a trailing-edge bend of 10° and twist of 6°.

Overall, the twist-compounded flexible-blade design outperformed both the standard and flexible turbines, delivering higher torque and improved efficiency across a range of airflow conditions. While effective, the flexible blades exhibited spanwise bending and elongation at high speeds, indicating the need for further material optimization. These findings demonstrate that adaptive blade flexibility and vortex control are effective strategies for improving Wells turbine performance, with potential applications in both wave and wind energy systems.

Nomenclature

A Lift force (N)
c Chord length of turbine blade (m)
C_l Lift coefficient
C_d Drag coefficient
D Drag force (N)
D_{tip} Turbine blade tip diameter (m)
D_{hub} Turbine hub diameter (m)
h Blade height (m)
ID Turbine casing inside diameter (m)
m Mass flow rate (kg/s)
n Number of blades
N Turbine speed (rpm)
P Static pressure (N/m²)
p_0 Stagnation pressure (N/m²)
P Power (W)
Q Volume flow rate (m³/s)
S Spacing between turbine blades (m)
T Thrust (N)
U Blade speed (m/s)
V_1 Absolute air velocity at blade inlet (m/s)
V_2 Absolute air velocity at blade exit (m/s)
V_a Axial air velocity (m/s)
V_m Absolute mean air velocity with respect to blade (m/s)
V_{u1} Absolute air velocity projected onto U at inlet of blade (m/s)
V_{u2} Absolute air velocity projected onto U at exit of blade (m/s)
W_1 Relative air velocity at inlet of turbine blade (m/s)
W_2 Relative air velocity at exit of turbine blade (m/s)

Greek symbols

α_1 Inlet angle of absolute velocity (deg)
α_2 Exit angle of absolute velocity (deg)
α_m Mean incident angle (deg)
β_1 Inlet angle of relative velocity (deg)
β_2 Exit angle of relative velocity (deg)
ρ Density of air (kg/m³)
ω Turbine angular speed (rad/s)
η_a Aerodynamic efficiency
Φ Flow ratio (Va / U)

References

[1] Raghunathan, S. “The Wells Turbine for Wave Energy Conversion.” Prog. Aerospace Sci., 17 Jan. 1995: 335–386.

[2] Gato, L. M. C., and Falcão, A. F. de O. “Aerodynamics of the Wells Turbine.” Int. J. Mech. Sci., 22 Jan. 1988: 383–395.

[3] European Energy Commission Atlas Website. “Wave Energy – Current Market Position.” http://ec.europa.eu/energy/atlas/html/wavpost3.html (accessed September 2006).

[4] Raghunathan, S., Setoguchi, T., and Kaneko, K. “Some Techniques to Improve the Range of the Wells Turbine for Wave Power Generation.” J. of Turbomachinery, 22 Mar. 1988: 792–795.

[5] Triantafyllou, M. S., Techet, A. H., Zhu, Q., Beal, D. N., Hover, F. S., and Yue, D. K. P. "Vorticity Control in Fish-like Propulsion and Maneuvering." Society for Integrative and Comparative Biology, 2002.
[6] How Fish Swim, Florida Museum https://www.floridamuseum.ufl.edu/discover-fish/fish/how-fish-swim/, accessed December 2025
[7] Dhananjay Mangalekar, a Flexible Free Vortex Turbine Blade: Design and Analysis at Part-Load, Master's Thesis, 2007, Department of Mechanical Engineering, San Diego State University
[8] Dixon, S. L. "Three-Dimensional Flows in Axial Turbomachines." In Fluid Mechanics, Thermodynamics of Turbomachinery, 3rd ed., 152–159. Pergamon Press Ltd., 1978.
[9] Horlock, J. H. "Three-Dimensional Cascades." In Axial Flow Turbines, 148–151. London: Butterworths, 1966.